

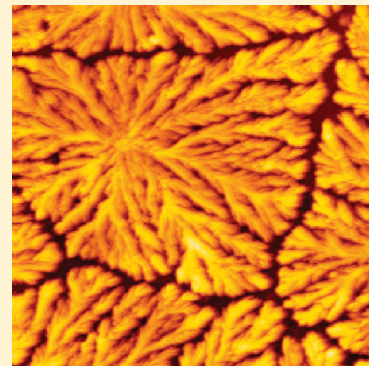
Insight into Fractal Self-Assembly of Poly(diallyldimethylammonium chloride)/Sodium Carboxymethyl Cellulose Polyelectrolyte Complex Nanoparticles

Qiang Zhao, Quanfu An,* Jinwen Qian, Xuesan Wang, and Yang Zhou

MOE Key Laboratory of Macromolecule Synthesis and Functionalization, Department of Polymer Science and Engineering, Zhejiang University, Hangzhou 310027, P.R. China

 Supporting Information

ABSTRACT: Poly(diallyldimethylammonium chloride)-sodium carboxymethyl cellulose polyelectrolyte complexes (PDDA-CMCNa PECs) solids were prepared and dispersed in NaOH aqueous solution. Self-assembly of PECs nanoparticles during the solvent evaporation was examined by field emission electron microscopy (FESEM), atomic force microscopy (AFM), and fractal dimension analysis. It was found that tree-shaped fractal patterns formed after the solvent (water) was dried at ambient temperatures, and the fractal pattern is composed of needle-shaped PEC aggregate (PECA) nanoparticles. Time-dependent FESEM observation revealed that the fractal pattern started with the formation of initial nucleon and it is growing, during which the diffusion limited aggregation (DLA) mechanism revealed and made the pattern branched. Physical insight into the DLA mechanism was discussed in detail. Effects of PEC concentrations, PEC compositions, solvent evaporation temperatures, pH of PEC dispersion, and chemical structures of PECs on the formation of self-assembled fractal pattern were studied. Generally, it was found that the morphologies, charge characters of PEC particles, and the solvent evaporation conditions play important roles during the fractal self-assembly process.



INTRODUCTION

Polyelectrolyte complexes (PECs), which are formed due to the ionic interaction between oppositely charged polyelectrolytes, are gaining increasing interest from both the material and chemistry points of view.^{1–11} PECs are usually studied in forms of aqueous dispersions and have various applications such as gene and drug delivery, flocculants, paper strengthening, coatings, gels, microencapsulation, and so on. Currently, common methods for preparing PEC dispersions include stoichiometric^{10–14} and nonstoichiometric mixing methods.^{15–20} Both methods mix two oppositely charged polyelectrolyte solution, and obtain PEC dispersions *in situ*. As prepared PEC dispersions are composed of PEC aggregate (PECA) nanoparticles, and their stability in the dispersion depends on the mixing ratio of component polyelectrolytes and charge density of PEC particles. Recently, we proposed a new method for preparing PECs dispersions by utilizing solution processable PECs, which were prepared via a so-called “protection deprotection” method.^{21–25} This method paves the way for exploring functionalities and applications of PEC solids, and provides a new type of self-assembly building block. For instance, homogeneous PEC membranes made from these processable PECs showed highly improved performance both in pervaporation^{21–23} and nanofiltration.²⁵ Moreover, drying the as prepared PEC dispersions at ambient conditions produces fractal patterns,²⁶ which have not been reported with any other PECs dispersions that were prepared via the solution mixing method.^{1–20} In our previous study,²⁶ it was mainly

reported that the fractal self-assembly is not just an occasional case but happens with four processable PECs prepared via our method. However, both the fractal self-assembly mechanism and its dependence on various external and inner factors have not been discussed thoroughly. Obviously, exploring both the mechanism and more details of this fractal self-assembly phenomenon is desired to gain deeper physical insight.

The concept of fractals was first introduced by Mandelbrot in 1970s,²⁷ and it constitutes a family of interesting nonlinear shapes. Recently, fractal patterns of polymers have attracted great interest.^{28–43} This is because fractal patterns usually form in nonequilibrium conditions that are much closer to real applications. For instance, nonequilibrium crystallization of polymers such as poly(ϵ -caprolactone),²⁸ poly(ethyl oxide),^{29–31} polymethyl methacrylate^{32,33} and isotactic poly(styrene)^{34,35} can produce fractal or dendritic crystalline morphologies. Besides this, supramolecular self-assembly, freezing-drying, and hybrid annealing of polymers can also produce fractal patterns.^{36–42} More recently, Haidara and co-workers reported that sodium alginate (SA) can form fractal pattern via the counterions mediated crystallization during solvent evaporation.⁴³ This result is interesting because pristine SA is basically noncrystalline. However, it is obvious that the processes of fractal pattern

Received: May 1, 2011

Revised: November 12, 2011

Published: November 18, 2011

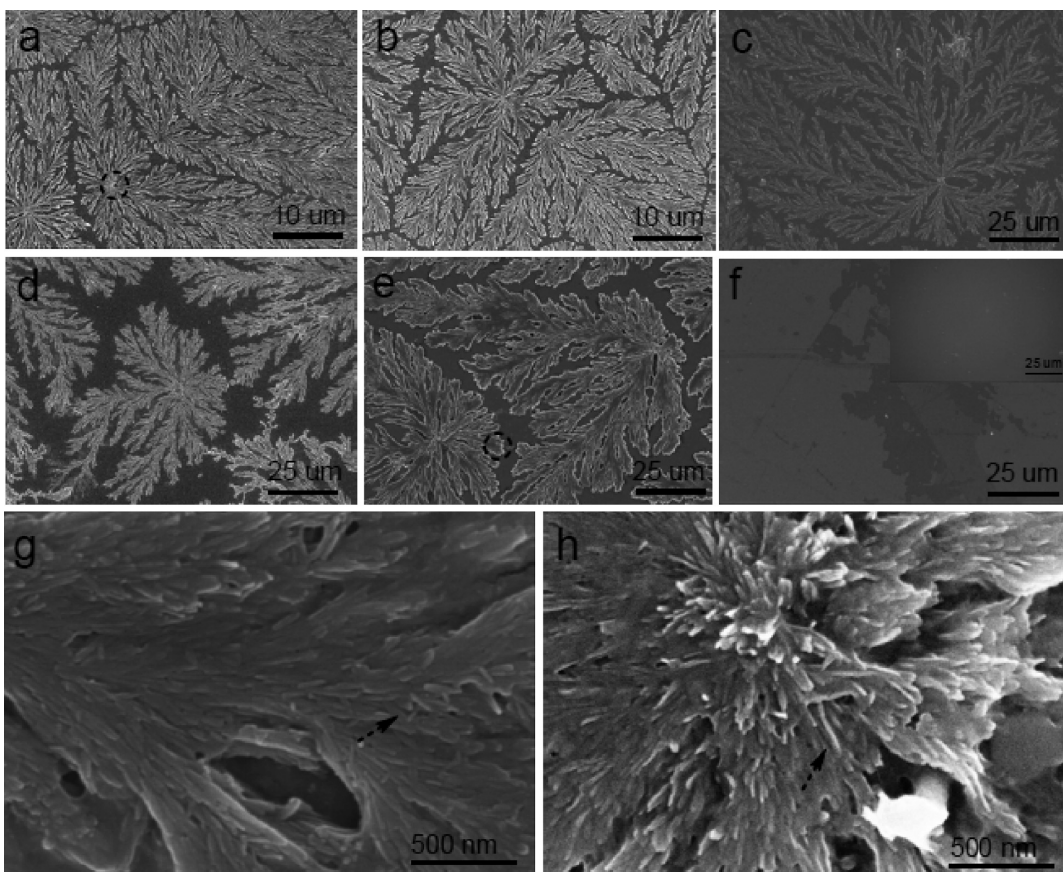


Figure 1. Pattern of (a) PEC0.15; (b) PEC 0.19; (c) PEC0.28; (d) PEC0.38; (e) PEC0.63; (f) CMCNa and PDPA (inset of f), (g,h) magnified observation of the marked region in (a) and (e), respectively;. The concentration of all PEC dispersion, CMCNa, and PDPA solution is 0.02 wt %, and solvent evaporation temperature is 30 °C.

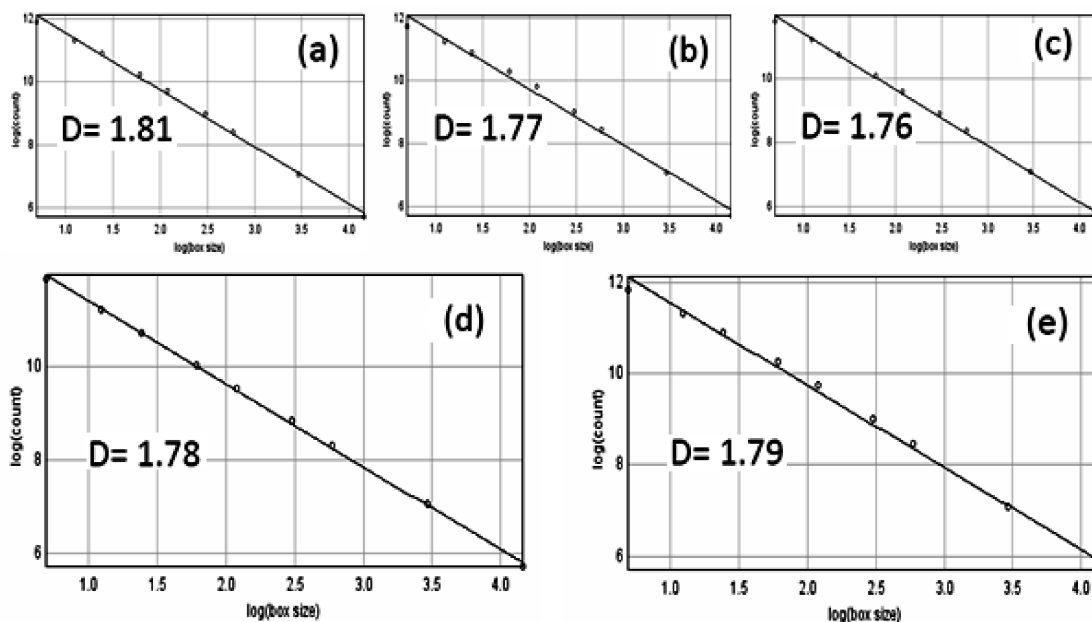


Figure 2. Fractal dimension of the pattern (a) PEC0.15, (b) PEC 0.19, (c) PEC0.28 (d) PEC0.38 (e) PEC0.63. The micrographs used for calculating fractal dimensions were those shown in Figure 1a–e, respectively.

formation deserve more studies. Especially, fractal patterns of polymers that are not driven by crystallization are less studied.

In this study, we move on to study the fractal pattern formation of PEC dispersions on water–silicon wafer interface.

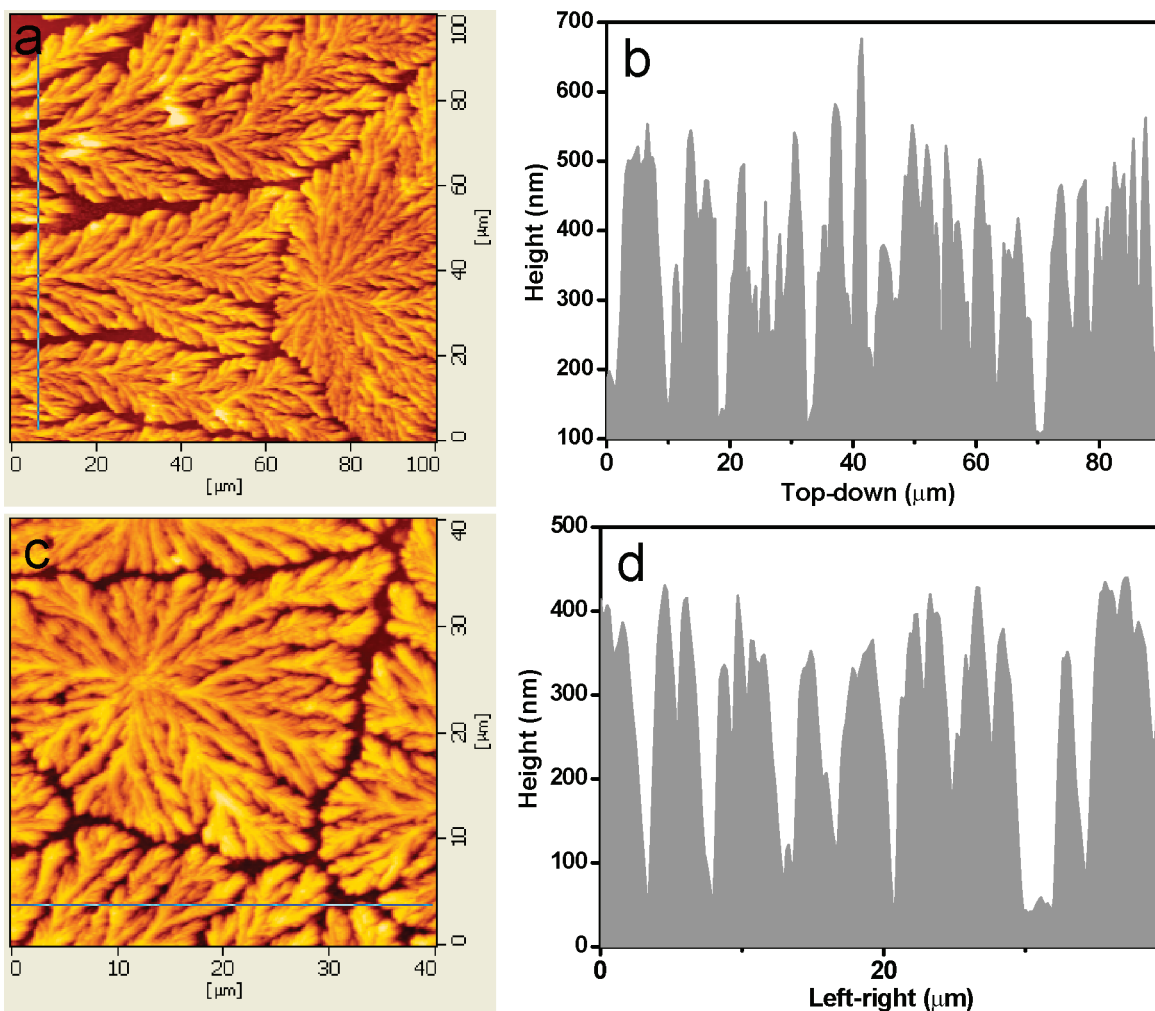


Figure 3. (a,c) AFM micrographs of the fractal pattern of PEC0.38 and PEC0.63, respectively. (b,d) Height profile of the marked line in (a) and (c), respectively. The PEC concentration is 0.02 wt %, and solvent was dried on a silicon wafer at 30 °C.

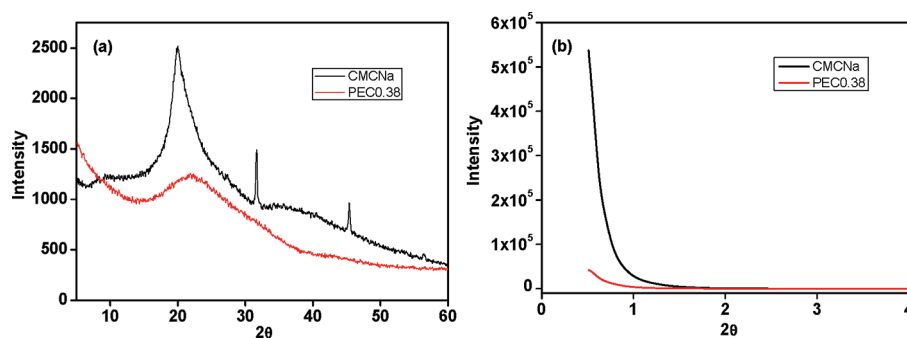


Figure 4. (a) WAXD and (b) SAXS curves of CMCNa and PEC0.38 films.

The aim of this work is to study the structure, formation mechanism, and tuning of the PEC fractal self-assembly process. Physical insight into the mechanism of fractal self-assembly is discussed on the basis of diffusion limited aggregation (DLA) model. Effect of PEC composition, PEC concentration, pH of the PEC dispersion, solvent evaporation temperature and chemical structures of PEC nanoparticles on the pattern formation of PECs is studied. This work includes two parts, the first of which studies structures of PEC fractal pattern. The second part

deals with the mechanism of fractal pattern formation and its tailoring.

EXPERIMENTAL SECTION

Materials. Poly(diallyldimethylammonium chloride) (PDDA) ($M_w = 100\,000\text{--}200\,000$ g/mol, 20 wt % aqueous solution) was purchased from Aldrich and used without further purification. Sodium carboxymethyl cellulose (CMCNa) (degree of substitution:

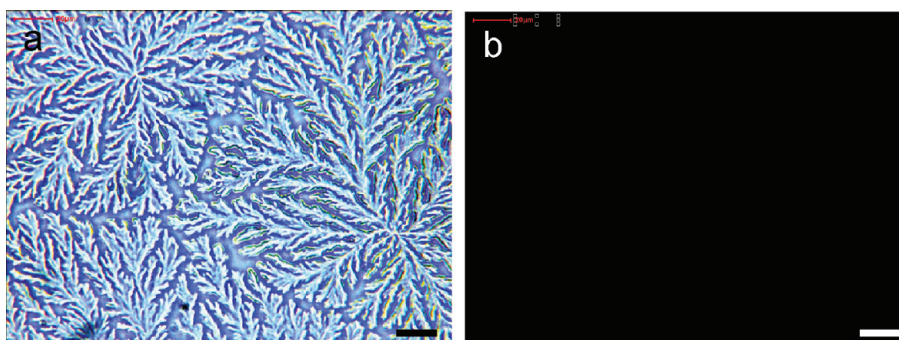


Figure 5. CMCNa-PDDA PEC0.38 fractals observed under (a) optical microscopy and (b) POM with polarizer and analyzer perpendicular to each other. Scale bars are all $20\ \mu\text{m}$, and PEC dispersion (0.2 wt %) was dried at $30\ ^\circ\text{C}$.

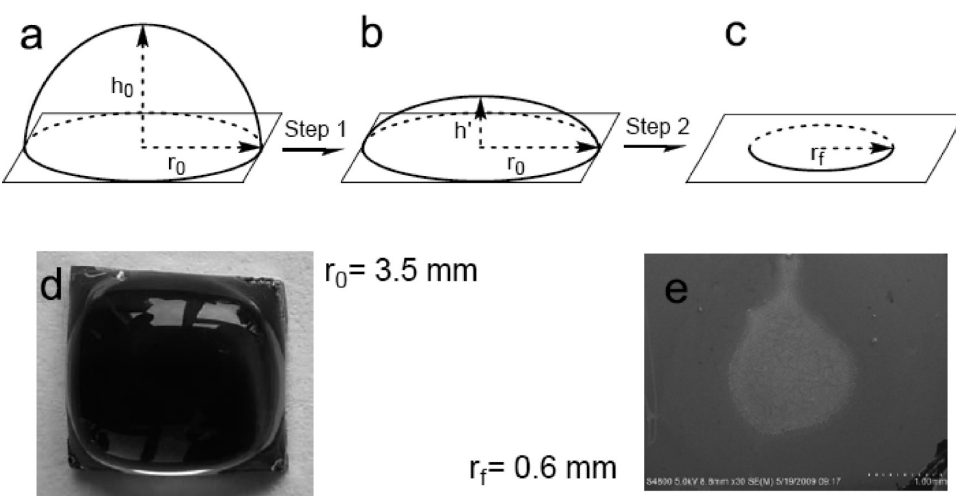


Figure 6. (a–c) Schematic model of drying PEC dispersion ($t = t_0$, $t = t_c$, and $t = t_b$ respectively). (d) Optical photographs of the initial drop of PEC0.38 dispersions (0.02 wt %) on a silicon wafer. (e) FESEM examinations after (d) was dried.

0.85) was purchased from Sinopharm Chemical Reagent Co., Ltd, Shanghai, China. The intrinsic viscosity of CMCNa in 0.01 M NaCl at $30\ ^\circ\text{C}$ is $1198.3\ \text{mL/g}$ by the extrapolation method according to Huggins viscosity equation $\eta_{sp}/c = [\eta] + k_H[\eta]^2c$ (Figure S1, Supporting Information). PECs made of PDDA and CMCNa (PDDA-CMCNa PECs) were prepared according to the so-called “protection deprotection” method we reported previously^{21–25} (Figure S2, Supporting Information). The compositions of PECs are expressed by the mole ratio of PDDA monomers to CMCNa monomers ($M_{\text{PDDA}}:M_{\text{CMCNa}}$). In this study, PDDA-CMCNa PECs with $M_{\text{PDDA}}:M_{\text{CMCNa}}$ values of 0.63, 0.38, 0.28, 0.19, 0.15 were prepared and referred to as PEC0.63, PEC0.38, PEC0.28, PEC0.19, and PEC0.15, respectively (Table S1, Supporting Information).

Fractal Self-Assembly of PECs. PECs solids were dispersed in NaOH aqueous solution because there are COOH groups in the PECs. Note that the NaOH mole concentration for dissolving PEC is dependent on the COOH amount in the PECs, and is not excessive. Hence, pH values of PEC dispersions, otherwise stated, are maintained at 8. PEC aqueous dispersion (0.06 mL) was deposited on a silicon wafer ($7 \times 7\ \text{mm}^2$), and the solvent (water) was evaporated for 24 h at designed temperatures. Patterns form on the silicon wafer during the solvent evaporation. In this study, effects of experimental parameters such as PEC concentrations, PEC compositions, solvent evaporation temperatures, pH values, and chemical structures of the PEC dispersions on their pattern formation were studied.

Characterizations. Field emission electron scanning (FESEM) examination was performed on a Hitachi S4800 microscope. Patterns on silicon wafers were coated with gold nanoparticles for 30 s prior to FESEM examinations. Atomic force microscopy (AFM) (tapping mode) was operated on a Seiko SPI3800N station (Seiko Instruments Inc.). Silicon tips (NSG10, NT-MDT) with a resonance frequency of ca. 330 kHz were used. Polarizing optical microscopy (POM) was performed on an Olympus BX51 microscopy at $25\ ^\circ\text{C}$. For POM characterization, PEC dispersion (0.2 wt %) was deposited on glass slides, dried at $30\ ^\circ\text{C}$, and examined by POM. Wide-angle X-ray diffraction (WAXD) was performed on an X-ray diffractometer (XD-98, Philips X light pipe), and CuK α was utilized for X-rays sources. Small-angle X-ray scattering (SAXS) was performed with an X'PERT-PRO MPD by using CuK α ($\lambda=1.5405\ \text{\AA}$) as radiation. The fractal dimensions of these patterns were obtained by Image-J software by using the box-counting method, using the box-counting algorithm with box values of 2, 3, 4, 6, 8, 12, 16, 32, and 64.⁴⁴ Note that patterns that are obviously not fractals were not measured by Image-J software.

RESULTS AND DISCUSSION

Figure 1 shows the FESEM examination of drying PEC0.15, PEC0.19, PEC0.28, PEC0.38, PEC0.63, CMCNa, and PDDA solutions (0.02 wt %) at $30\ ^\circ\text{C}$ on silicon wafers. It is seen that

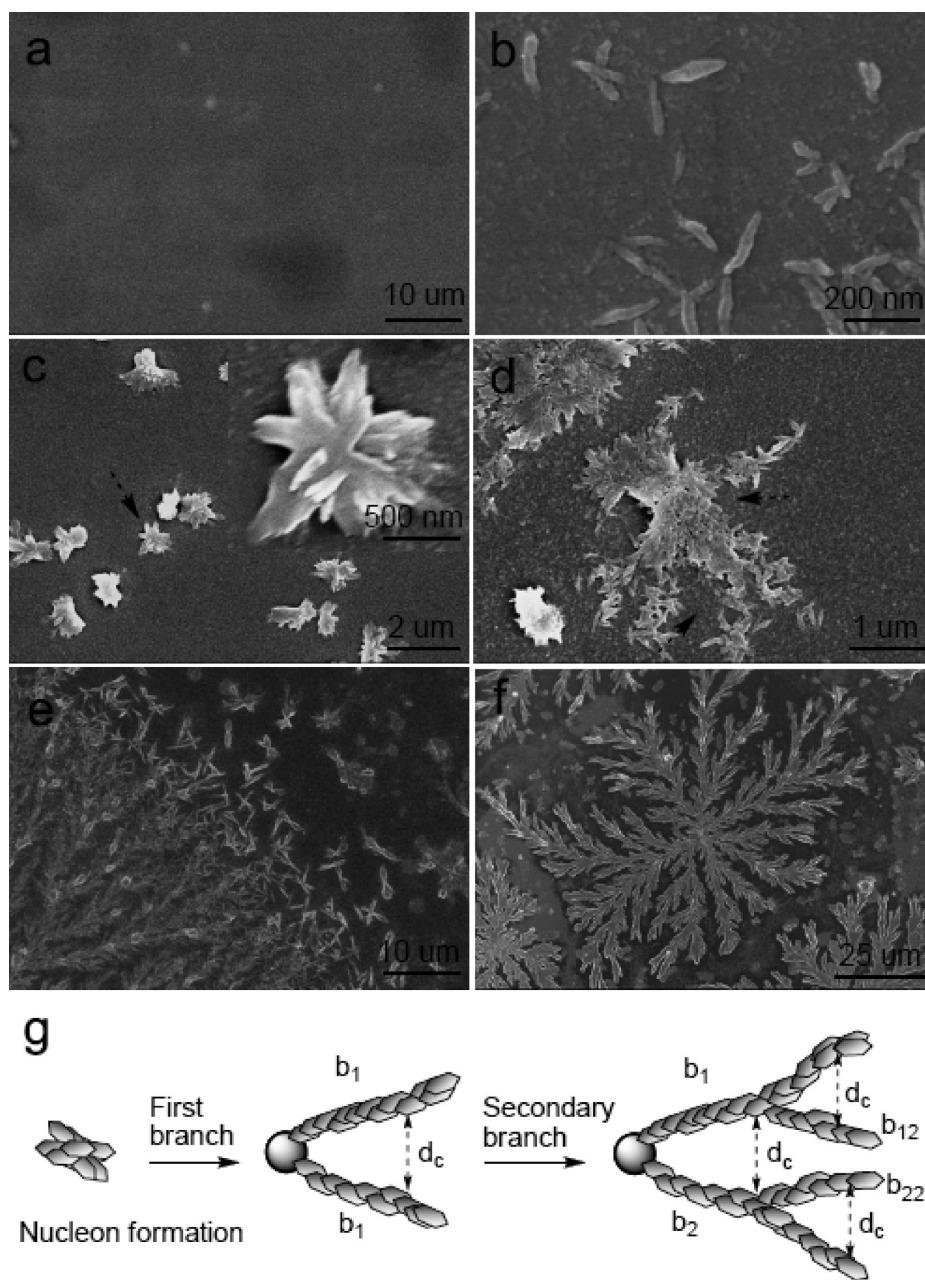


Figure 7. Quasi real-time FESEM observation of PEC0.38 fractal tree formation with different solvent evaporation time: (a) 190 min, (b) 200 min, (c) 210 min, (d) 220 min, (e) 230 min, and (f) 240 min. PEC0.38 concentration: 0.02 wt %, solvent was dried on silicon wafers at 30 °C. Figure 6g is a schematic illustration of the diffusion limited mechanism.

patterns of the five PECs dispersions with different compositions are similar to each other. That is, branched and self-similar patterns (referred to as fractal “trees”) are obtained with all PECs (Figures 1a–e). It should be noted that fractal trees in Figure 1 are not as strictly self-similar at all scales as that of mathematically defined fractals such as the Kohn curve and Sierpinski’s hexagonal gasket.²⁷ Instead, they grow up cooperatively from a central nucleus, forming distinct borders among different fractal trees. Moreover, both the component polyelectrolytes of CMCNa and PDDA show no such fractal pattern under the same experimental conditions (Figure 1f and its inset). Figure 1g,h further shows that PEC fractal trees are composed of needle-shaped nanostructures. Transmission electron microscopy

(TEM) observations also support that PEC particles are needle-shaped. (Figure S4, Supporting Information). These nanostructures are PECA particles, which are composed of PDDA and CMCNa chains binding via ionic interaction.²¹ Sizes of PECA nanoparticles, as shown in Figure 1g,h, are ca. 50 nm in width and 300 nm in length. Considering that both CMCNa and PDDA show no fractal patterns, it is speculated that the formation of PECA particles is a key step for the fractal pattern formation. Moreover, in literature, drying other PEC dispersions show no such fractal patterns.^{10–20} Thus, the needle-shaped morphology of PECA particles may play an important role for fractal pattern formation. More recently, Wang and co-workers found that rod shaped peptides as building blocks can also form fractal patterns via

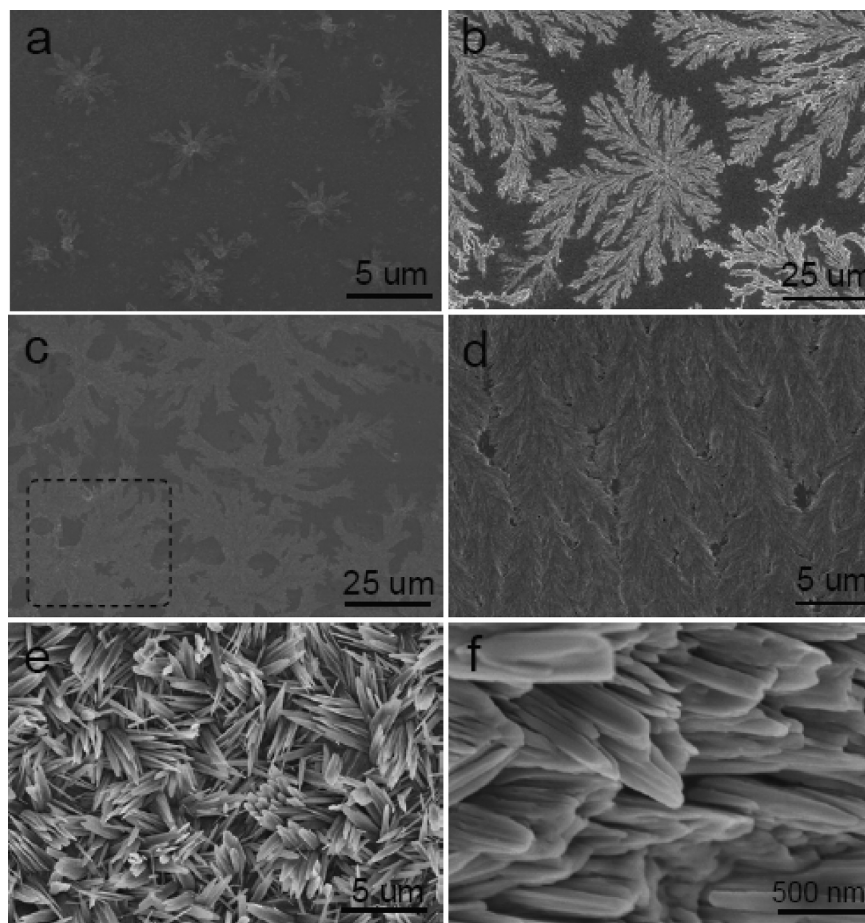


Figure 8. Pattern of PEC0.38 dispersion dried on silicon wafers at 30 °C: (a) 0.005 wt %, (b) 0.02 wt %, (c) 0.1 wt %, (d) 0.5 wt %, and (e) 2 wt %. (f) Cross-section of (e).

self-assembly.⁴² Probably, the linear shape of nanoparticles is more easy for ordered and aligned packing. Figure 2 shows that fractal dimensions of fractal trees in Figures 2a–e are in the range of 1.76–1.81, suggesting that the formation of these fractal trees may obey the DLA model.^{45–47}

Structures of PEC fractal trees were further characterized by AFM (Figure 3). Fractal trees in Figure 3a and Figure 3c are identical with that observed in Figure 1a–e. That is, both fractal trees are branched, self-similar and grow from center nucleus. AFM height profiles (Figure 3b and 3d) show that the average thickness of PEC fractal trees is ca. 350 nm above the silicon wafer. This thickness indicates that fractal trees are not composed of a single layer of PECA particles because the thickness of a single PECA is only ca. 50 nm. For fractal patterns obtained by nonequilibrium of polymers, their thicknesses are usually below 10 nm.^{28–33} Moreover, the height profile in Figure 3b and Figure 3d is V shaped along the perpendicular direction. This feature is associated with the fractal tree formation mechanism and will be discussed in later sections.

Figures 1–3 characterize the structures of PEC fractal trees, showing that they are composed of needle-shaped PECA particles. Regarding the formation of PEC fractal patterns, the first thing to consider is whether they are formed via the crystallization of PEC because crystallization seems to be the most frequent driving force for producing fractal patterns.^{28–35,43} However, it is has been known that PECs are generally

noncrystalline due to their ionic cross-linking structures.^{1,3,48} To clarify this issue, both the X-ray scattering and polarized light microscopy were utilized to characterize structures of PECs. From WAXD curves (Figure 4a), it is seen that CMCNa is semicrystalline, and this is due to the ordered packing of CMCNa chains caused by hydrogen bonding. On the contrary, PEC0.38 is generally noncrystalline, which is because the ionic cross-linking between CMCNa and PDDA chains inhibited their chain mobility and ordered packing.¹ Moreover, XRD peak of NaCl is not seen from WAXD curve of PEC0.38, indicating that PECs are basically free from NaCl salts. Moreover, no obvious peaks are seen on SAXS curves of both PEC0.38 and CMCNa, indicating that there are no crystalline phases or large-scale ordered structures in them. Actually, in our previous study, we've found that another four PECs prepared via the same “protection deprotection” method were all noncrystalline.²⁶ Meanwhile, POM observation of PEC fractals under cross polarized light shows a totally black image (Figure 5b), supporting that these fractals are generally noncrystalline. On the basis of these results, the fractal pattern formation of PECs is studied from the kinetic point of view.

Figure 6a–c schematically describes the drying process of PEC dispersions on a silicon wafer. A quasi hemisphere (height: h_0) is formed when 0.06 mL of PEC dispersion is deposited on a silicon wafer ($7 \times 7 \text{ mm}^2$). The contacting line between the hemisphere and silicon wafer is a circle (diameter: r_0). Then, the

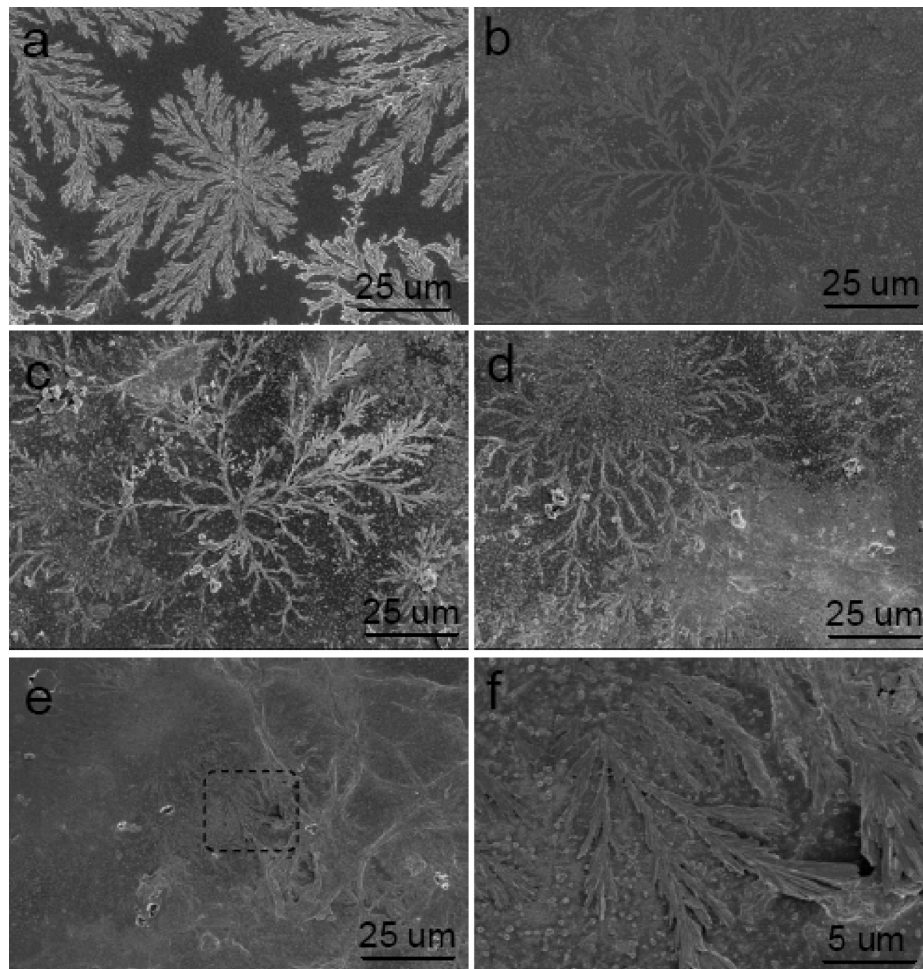


Figure 9. Fractal pattern of PEC0.38 dispersion dried at different temperatures on silicon wafers: (a) 30 °C, (b) 40 °C, (c) 50 °C, (d) 60 °C, (e) 70 °C. (f) Marked region in (e). The PEC concentration is all 0.02 wt %.

drying of the PEC dispersion involves two steps with increasing drying time. First, h_0 decreases while r_0 does not change until a critical drying time of t_c . Second, both the h' and r_0 decreases with increasing drying time, during which the contacting line begins to contract macroscopically. The shape of the final contacting region is nearly a round circle, and its radius is defined as r_f . Figure 6d and Figure 6e show that the r_0 and r_f are about 3.5 mm and 0.6 mm, respectively, confirming that the drop of PEC aqueous dispersion indeed contracts during the solvent evaporation. It should be noted that fractal trees are formed within r_f .

Figure 7 shows the time-dependent FESEM examination of drying PEC0.38 dispersion (0.02 wt %) at 30 °C. In Figure 7a, no PECA particles are observed on the silicon wafer until a drying time of 190 min. This is because 190 min are below the critical drying time of t_c and the contacting line does not contract before t_c . As a result, no PECA particles were trapped on the silicon wafer. In Figure 7b, the drying time reaches 200 min, and some PECA particles were trapped on the silicon wafer. This is because the drying time of 200 min probably surpasses the t_c , and the contacting line begins to contract. With further increasing the drying time, Figure 7c and its insertion show that PECA particles in the dispersion keep on adhering to the already trapped PECA particles and form the initial nucleon, which are

spindle shaped and composed of tens of PECA particles. The formation of initial nucleon broke the balance and made PECA particles preferentially adhere to them instead of to the silicon wafer surface. For example, Figure 7d and Figure 7e show that PECA particles cannot reach the region between two neighboring branches (dash arrow) because they were trapped by either branches before they can reach the silicon wafer. Then, the fractal trees kept growing and became branched due to the so-called DLA mechanism and screening effect.²⁷

Figure 7g shows a schematic diagram to illustrate the physical insight of the DLA mechanism and screening effect. PECA particles preferentially adhere to the initial nucleon via “random walk”, which causes the first generation of branches (b_1) to grow up from the nucleon. An energy barrier exists between two neighboring branches because PECA particles are likely charged. As a result of the energy barrier, PECA particles that move from perpendicular direction (z direction) of the silicon wafer cannot reach the concave region between two neighboring branches. The strength of the energy barrier decreases with increasing the distance (d) between two neighboring branches. Consequently, a critical distance (d_c) exists, above which PECA particles can break the energy barrier and reach the silicon wafer. In other words, a secondary generation of branches (b_{12}) will automatically grow from the “mother branch” (b_1) when $d > d_c$. The same

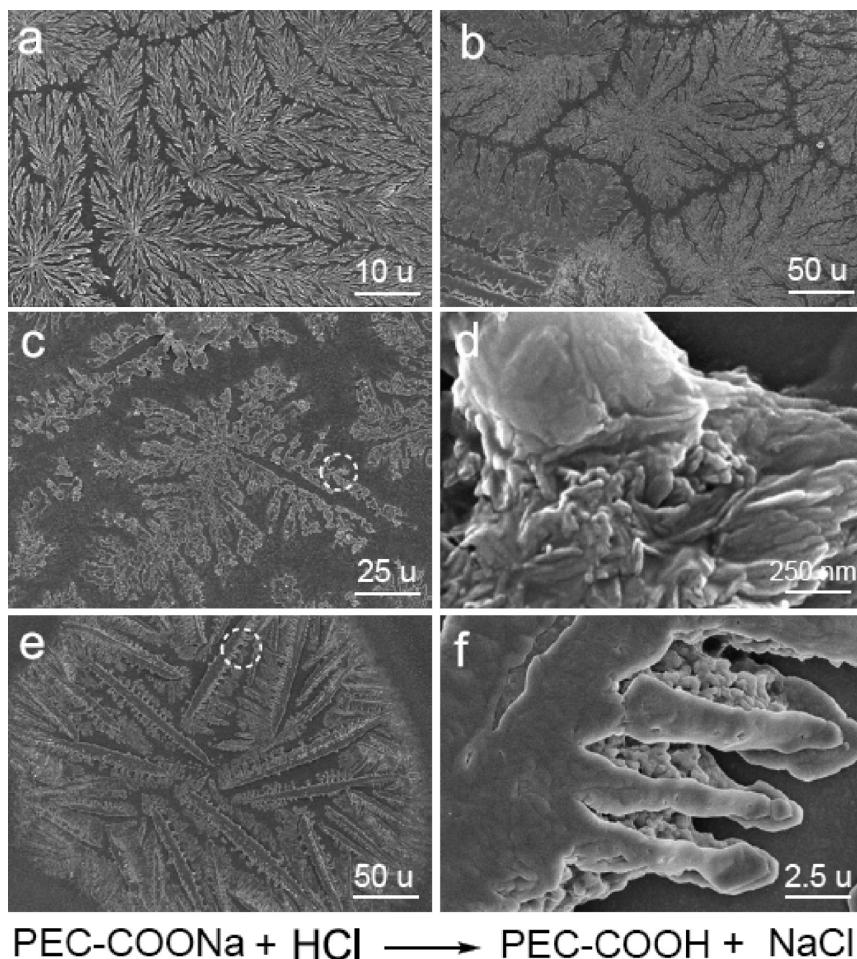


Figure 10. Effect of pH of PEC0.15 dispersions on their fractal tree formation: (a) pH = 8, (b) pH = 7, (c,d) pH = 6, (e,f) pH = 5.

principle is also applicable to the next generations of branches. Thus, the self-assembly pattern automatically becomes branched during the growing of the fractal trees. One may argue what guarantees the speculation that PECA particles move toward the fractal trees from the z direction. Height profiles in Figure 3 show "V"-shaped pits, indicating that the concaves between two neighboring branches are V-shaped. This feature supports the idea that PECA particles move toward the readily formed fractal trees from the z direction. Moreover, AFM height analysis show that fractal trees are not composed of a monolayer of PECA, which also supports the idea that PECA particles move toward fractal trees from the z direction.

Figure 8 shows the effect of PEC0.38 concentration on its fractal pattern formation at 30 °C. Sunflower-shaped or star-shaped fractals with a diameter of ca. 5 μm and well-grown fractal trees with diameters of ca. 100–500 μm are obtained when the PEC0.38 concentration increases from 0.005 to 0.02 wt %. With further increasing PEC0.38 concentration to 0.1 and 0.5 wt %, Figure 8c,d shows a morphology shift from separated fractals to dense branching morphology (DBM). That is, branches of different fractal trees bang into each other (rectangular region in Figure 8c) and are packed more tightly (Figure 8d). Finally, a dense PEC membrane is obtained when the concentration of PEC0.38 reaches 2 wt % (Figure 8e). Both the FESEM surface and cross-sectional (Figure 8f) examinations show that the dense PEC membrane is composed of needle-shaped PECA particles.

Noticeably, this type of PEC membrane shows very high separation performances,^{21–25,49} a feature that may be associated with the structures of PECA particles. The dependence of PEC assembly morphologies on their concentrations can be explained via the DLA model. At high PEC concentrations (above 0.1 wt % in this study), PECA particles are crowded, and they are not able to move freely in the dispersion via random walk. Hence, the energy barrier between neighboring branches failed to regulate the pattern growth, and dense branch morphologies were formed. Moreover, fractal dimensions of Figure 8a–c are 1.95, 1.79, and 1.91, respectively (Figure S6, Supporting Information), which are in accordance with their pattern morphologies.

Figure 9 shows the effect of drying temperatures on the fractal pattern formation of PEC0.38 dispersion (0.02 wt %). It is seen that the formation of fractal trees is gradually blocked with increasing temperatures from 30 to 70 °C (Figure 9a–g). Moreover, it seems that the increasing solvent evaporation temperature has a heavier effect on the formation of branches than on the central nucleus. For example, central nucleuses are formed until a temperature of 60 °C, while the growing of branches is blocked when temperature is above 40 °C. Water molecules evaporate faster with increasing temperatures (Figure S5, Supporting Information). Consequently, PECA particles gain a momentum big enough for breaking the energy barrier between neighboring branches and reaching the surface of the silicon wafer randomly. In

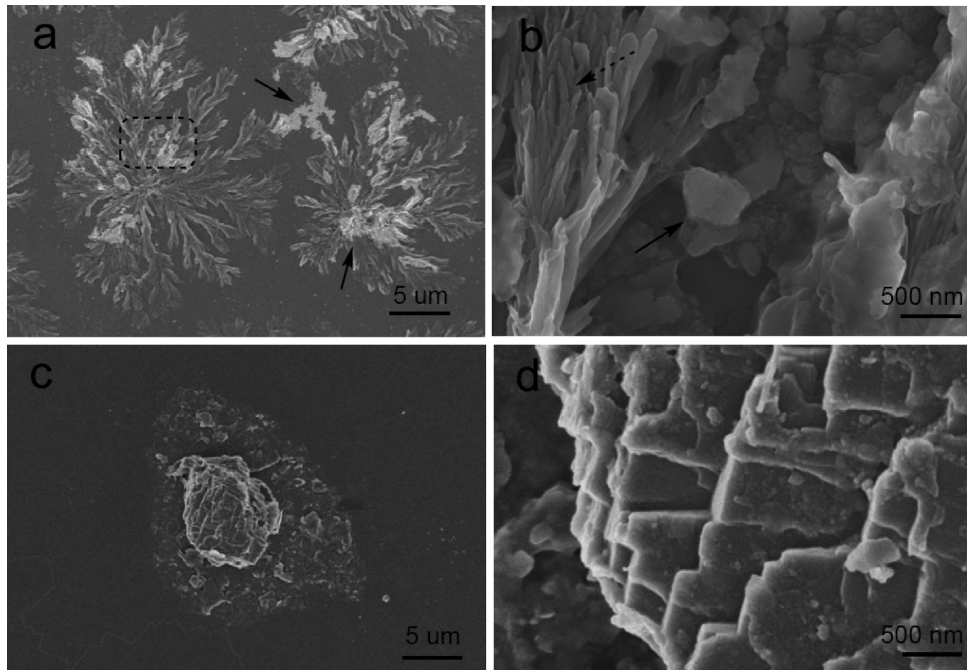


Figure 11. (a,b) Fractal self-assembly pattern of drying PEC0.15 dispersion added with 0.002 M NaCl. (c,d) Pattern of drying 0.002 M NaCl aqueous solution. PEC concentration: 0.02 wt %, drying temperature: 30 °C.

other words, the screening effect does not function at a higher temperature. Moreover, fractal dimensions of obtained patterns increase from 1.79 to 1.94 with increasing drying temperatures (Figure S7, Supporting Information). This result supports the discussion that the DLA mechanism and the shielding effect between PECA particles gradually lose function with increasing drying temperatures.

PEC0.15 was chosen to study the dependence of fractal pattern formation on pH values of their dispersions. This is because PEC0.15 has lower ionic complexation degree, and more COONa groups in their particles. Figure 10 shows the effect of pH values of PEC0.15 dispersion on its fractal tree pattern formation. It is seen that the fractal character of the pattern gradually disappears with decreasing pH. For instance, the pattern shifts from fractal (Figure 10a–c) to seaweed pattern (Figure 10e) when pH is decreased from 8 to 5. The COONa groups on PECA particles become protonated with decreasing pH³, which is supported by the decreasing zeta potential of PEC dispersions with decreasing their pH (Figure S9, Supporting Information). As a result, the energy barrier between two neighboring branches decreases and the screening effect gradually weakens. Consequently, fractal “trees” were not obtained at lower pH values. The magnified examinations in Figures 10d,f show that PECA particles adhered to each other, and this is because the charge repulsion force between two PECA particles decreases due to the protonation of COONa groups at lower pH values. In other words, the energy barrier between neighboring PEC branches decreases with decreasing pH values. Beside the protonation effect of HCl on PECA particles, it should be considered that the addition of HCl into PEC dispersions generated NaCl salts therein, and may influence their pattern formation as well. In order to clarify this issue, PEC0.15 dispersion (pH: ca. 8) added to 0.002 M of NaCl was dried at 30 °C to examine its pattern formation. It is seen from Figure 11 that a fractal pattern was obtained as well after the addition of 0.002 M NaCl. Moreover, as

indicated by arrows in Figure 11a, a layer of NaCl covered the fractal pattern. The magnified observation of the rectangular region of Figure 11a shows that the needle-shaped morphology of PECA particles (dashed arrow) remains. Figure 11c,d shows that drying 0.002 M NaCl alone does not generate a fractal pattern. Hence, Figure 11 indicates that the formation of a fractal pattern is not heavily influenced by NaCl.

Figure 12 shows self-assembly patterns of drying (30 °C) PDPA/CMCNa-g-PAN (PAN = polyacrylonitrile) PEC dispersions that contain different amounts of PAN side chains on CMCNa backbones. It is seen from Figure 12a–d that the fractal character of the obtained pattern gradually vanishes with increasing the PAN grafting amount from 10 wt % to 30 wt %. For instance, Figure 12b shows that the formation of PEC fractal trees is heavily blocked when the PAN grafting amount is above 10 wt %. Figure 12e–h shows the effect of PAN grafting amount on morphologies of corresponding PECA particles. It is seen from Figure 12e–h that the PECA particles gradually shift from needle-shaped morphology to round or globule-shaped morphologies with increasing PAN amount from 0 wt % to 30 wt %. Especially, Figure 12f shows that there are both needle/rod-shaped PECA particles and quasi-globule PECA particles at the PAN grafting amount of 10 wt %. It is well-known that PAN is not soluble in water. In CMCNa-g-PAN, the COONa groups on CMCNa chains provide the solubility in water while the hydrophobic association of PAN side chains make CMCNa-g-PAN macromolecules self-assemble into globule morphology in water. The more PAN side chains the CMCNa-g-PAN copolymer contains, the more compact conformation it adopts. As a result, the morphologies of PECA particles made from CMCNa-g-PAN and PDPA gradually shift from linear to globule shape. It is obviously more difficult for globule PECA particles to stack onto each other regularly for geometric reasons. Consequently, the DLA mechanism,

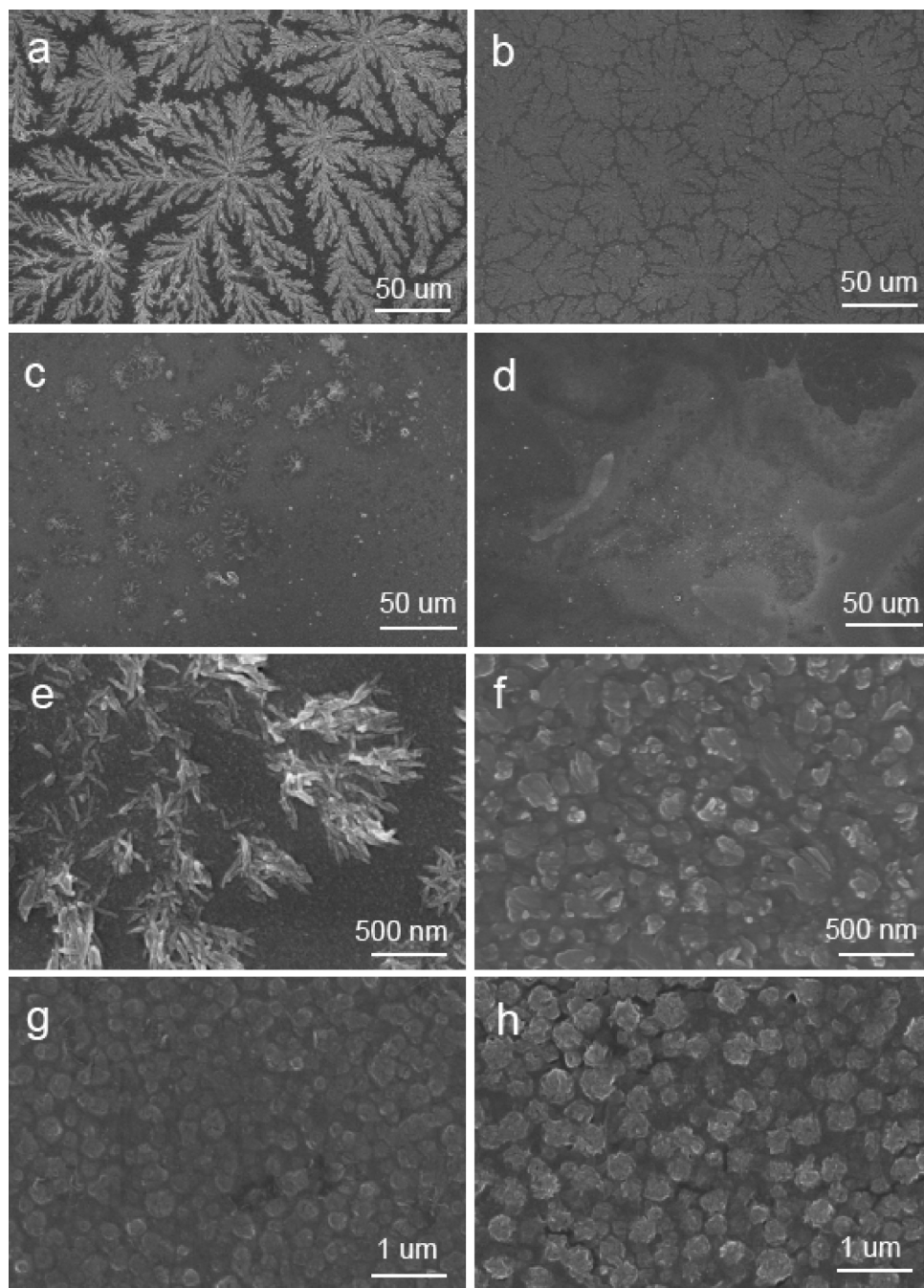


Figure 12. (a–d) Pattern of drying PDDA-CMCNa-g-PAN PEC dispersions that containing 0, 10, 20, 30 wt % of PAN, respectively, (e–h) morphologies of PECA particles in the PEC dispersions of (a–d), respectively. The drying temperature is 30 °C.

the screening effect, as well as the energy barriers vanish, and the growth of a fractal tree is blocked.

■ CONCLUSION

Fractal self-assembly of PDDA-CMCNa PECs nanoparticles during its solvent evaporation was studied in detail. Self-similar fractal patterns were obtained for PDDA-CMCNa PECs with five different compositions when drying their 0.02 wt % aqueous dispersions at 30 °C. FESEM and AFM show that the fractal pattern grows from a central nucleon and is composed of needle-shaped PECA particles that are formed due to the ionic

complexation between PDDA and CMCNa polyelectrolyte chains. Fractal dimensions of these fractal patterns are in the range of 1.76–1.81. Time-dependent FESEM observation shows that the fractal pattern started with the formation of initial central nucleon and grew via the adhering of PECA onto the nucleon. The branched character of the fractal pattern is due to the screening effect and DLA mechanism, both of which originated from the energy barriers between the likely charged PECA particles.

The tuning of PEC fractal self-assembly was studied. The pattern of PEC0.38 dispersions formed at 30 °C changed from tree-shaped fractals (0.005% and 0.02 wt %) to seaweed-like

pattern (0.5 wt %) and to dense membranes composed of needle-shaped PECAAs (2 wt %) upon increasing their concentrations. Moreover, both increasing the drying temperature and decreasing the pH of PEC dispersion blocked the formation of PEC fractal trees. This is because the energy barriers between PECA particles was either broken or reduced, both of which broke the screening effect or DLA mechanism. Grafting of hydrophobic PAN chains made PECA particles change from needle-like shape to globule shape, which also blocked the formation of fractal trees.

■ ASSOCIATED CONTENT

S Supporting Information. Synthesis and characterization of PDDA-CMCNa PECs and CMCNa-g-PAN copolymers. Dimensions of PEC fractal patterns. Weight loss curves of PEC dispersions (0.02 wt %) at different temperatures. This material is available free of charge via the Internet at <http://pubs.acs.org>.

■ AUTHOR INFORMATION

Corresponding Author

*Ph: (+86)-571-87953780; e-mail anqf@zju.edu.cn.

■ ACKNOWLEDGMENT

This research was financially supported by the NNSFC (51173160, 21106126, 50633030, 20876134) and the National Basic Research Program of China (2009CB623402), Fundamental Research Funds for the central University (The Engineering Research Center of Membrane and Water Treatment Technology, Ministry of Education), and Zhejiang Provincial Natural Science Foundation of China (No. Y4100250), National Science Foundation for Postdoctoral Scientists of China (No. 20100481412). The institute of chemistry, Chinese Academy of Sciences was acknowledged for help in SAXS measurements.

■ REFERENCES

- (1) Thünemann, A. F.; Müller, M.; Dautzenberg, H.; Joanny, J. F.; Löwen, H. *Adv. Polym. Sci.* **2004**, *166*, 113–171.
- (2) Sukhishvili, S. A.; Kharlampieva, E.; Izumrudov, V. *Macromolecules* **2006**, *39*, 8873–8881.
- (3) Tsuchida, E.; Abe, K. *Adv. Polym. Sci.* **1982**, *45*, 1–129.
- (4) Lee, Y.; Kataoka, K. *Soft Matter* **2009**, *5*, 3810–3817.
- (5) Hartig, S. M.; Greene, R. R.; Dikov, M. M.; Prokop, A.; Davidson, J. M. *Pharm. Res.* **2007**, *24*, 2353–2369.
- (6) Dragan, E. S.; Mihai, M. *ACS Appl. Mater. Interfaces* **2009**, *1*, 1231–1240.
- (7) Feng, X. H.; Pouw, K.; Leung, V.; Pelton, R. *Biomacromolecules* **2007**, *8*, 2161–2166.
- (8) Caruso, F.; Caruso, R. A.; Mohwald, H. *Science* **1998**, *282*, 1111–1114.
- (9) Shi, X. Y.; Shen, M.; Mohwald, H. *Prog. Polym. Sci.* **2004**, *29*, 987–1019.
- (10) Thünemann, A. F. *Macromolecules* **2000**, *33*, 5906–5911.
- (11) Thünemann, A. F.; Beyermann, J. *Macromolecules* **2001**, *34*, 6978–6885.
- (12) Zintchenko, A.; Dautzenberg, H.; Tauer, K.; Khrenov, V. *Langmuir* **2002**, *18*, 1386–1393.
- (13) Kabanov, A. V.; Bronich, T. K.; Kabanov, V. A.; Yu, K.; Eisenberg, A. *Macromolecules* **1996**, *29*, 6797–6802.
- (14) Kabanov, V. A. *Polym. Sci.* **1994**, *36*, 143–156.
- (15) Chelushkin, P. S.; Lysenko, E. A.; Bronich, T. K.; Eisenberg, A.; Kabanov, V. A.; Kabanov, A. V. *J. Phys. Chem. B* **2007**, *111*, 8419–8425.
- (16) Müller, M.; Reihs, T.; Ouyang, W. *Langmuir* **2005**, *21*, 465–469.
- (17) Müller, M.; Kessler, B.; Richter, S. *Langmuir* **2005**, *21*, 7044–705.
- (18) Stoerkle, D.; Duschner, S.; Heimann, N.; Maskos, M.; Schmidt, M. *Macromolecules* **2007**, *40*, 7998–8006.
- (19) Strand, S. P.; Danielsen, S.; Christensen, B. E.; Vårum, K. M. *Biomacromolecules* **2005**, *6*, 3357–3366.
- (20) Maurstad, G.; Danielsen, S.; Stokke, B. T. *J. Phys. Chem. B* **2003**, *107*, 8172–8180.
- (21) Zhao, Q.; An, Q. F.; Qian, J. W.; Sun, Z. W.; Lee, K. L.; Gao, C. J.; Lai, J. Y. *J. Phys. Chem. B* **2010**, *114*, 8100–8106.
- (22) Zhao, Q.; Qian, J. W.; An, Q. F.; Yang, Q.; Zhang, P. *J. Membr. Sci.* **2008**, *320*, 8–12.
- (23) Zhao, Q.; Qian, J. W.; Zhu, M. F.; An, Q. F. *J. Mater. Chem.* **2009**, *19*, 8732–8740.
- (24) Zhao, Q.; Qian, J. W.; An, Q. F.; Du, B. Y. *J. Mater. Chem.* **2009**, *19*, 8448–8455.
- (25) Ji, Y. L.; An, Q. F.; Zhao, Q.; Chen, H. L.; Qian, J. W.; Gao, C. J. *J. Membr. Sci.* **2010**, *357*, 80–89.
- (26) Zhao, Q.; Qian, J. W.; Gui, Z. L.; An, Q. F.; Zhu, M. H. *Soft Matter* **2010**, *6*, 1129–1137.
- (27) Mandelbrot, B. B. *Fractals: Form, Chance and Dimension*, Freeman: San Francisco, CA, 1977.
- (28) Mareau, V. H.; Prud'homme, R. E. *Macromolecules* **2005**, *38*, 398–408.
- (29) Zhai, X.; Wang, W.; Ma, Z.; Wen, X.; Yuan, F.; Tang, X.; He, B. L. *Macromolecules* **2005**, *38*, 1717–1722.
- (30) Zhai, X.; Wang, W.; Zhang, G.; He, B. L. *Macromolecules* **2006**, *39*, 324–329.
- (31) Ma, Z. P.; Zhang, G. L.; Zhai, X. M.; Jin, L. X.; Tang, X. F.; Yang, M.; Zheng, P.; Wang, W. *Polymer* **2008**, *49*, 1629–1634.
- (32) Granasy, L.; Pusztai, T.; Borzsonyi, T.; Warren, J. A.; Douglas, J. F. *Nat. Mater.* **2004**, *3*, 645–650.
- (33) Wang, M.; Braun, H. G.; Meyer, E. *Macromolecules* **2004**, *37*, 437–445.
- (34) Taguchi, K.; Miyaji, H.; Izumi, K.; Hoshino, A.; Miyamoto, Y.; Kokawa, R. *Polymer* **2001**, *42*, 7443.
- (35) Beers, K. L.; Douglas, J. F.; Amis, E. J.; Karim, A. *Langmuir* **2003**, *19*, 3935–3940.
- (36) Newkome, G. R.; Wang, P.; Moorefield, C. N.; Cho, T. J.; Mohapatra, P. P.; et al. *Science* **2006**, *312*, 1782–1785.
- (37) Lomander, A.; Hwang, W.; Zhang, S. *Nano Lett.* **2005**, *5*, 1255–1260.
- (38) Lee, I.; Ahn, J. S.; Hendricks, T. R.; Rubner, M. F.; Hammond, P. T. *Langmuir* **2004**, *20*, 2478–2483.
- (39) Tan, C. H.; Ravi, P.; Dai, S.; Tam, K. C. *Langmuir* **2004**, *20*, 9901–9904.
- (40) Gao, L. C.; Shi, L. Q.; An, Y. L.; Zhang, W. Q.; Shen, X. D.; Guo, S. Y.; He, B. L. *Langmuir* **2004**, *20*, 4787–4790.
- (41) Ramanathan, M.; Darling, S. B. *Soft Matter* **2009**, *5*, 4665–4671.
- (42) Wang, W. P.; Chau, Y. *Soft Matter* **2009**, *5*, 4893–4898.
- (43) Haidara, H.; Vonna, L.; Vidal, L. *Macromolecules* **2010**, *43*, 2421–2429.
- (44) Murr, M. M.; Morse, D. E. *Proc. Natl. Acad. Sci. U.S.A.* **2005**, *102*, 11657–11662.
- (45) Witten, T. A.; Sander, L. M. *Phys. Rev. Lett.* **1981**, *47*, 1400–1403.
- (46) Witten, T. A.; Sander, L. M. *Phys. Rev. B* **1983**, *27*, 5686–5697.
- (47) Rothenbuhler, J. R.; Huang, J. R.; DiDonna, B. A.; Levine, A. J.; Mason, T. G. *Soft Matter* **2009**, *5*, 3639–3645.
- (48) Zhao, Q.; An, Q. F.; Ji, Y. L.; Qian, J. W.; Gao, C. J. *J. Membr. Sci.* **2011**, *379*, 19–45.
- (49) Jin, H. T.; An, Q. F.; Zhao, Q.; Qian, J. W.; Zhu, M. H. *J. Membr. Sci.* **2010**, *347*, 183–192.